An Experimental Study of the Influence of the Preflush Salinity on Enhanced Oil Recovery Using Silica-Based Nanofluids

Tola Sreu [1,*], Kyuro Sasaki [1,2], Yuichi Sugai [1] and Ronald Nguele [1]

[1] Resources Production and Safety Engineering Laboratory, Department of Earth Resources Engineering, Faculty of Engineering, Kyushu University, Fukuoka 819-0395, Japan; krsasaki@hotmail.com (K.S.); sugai@mine.kyushu-u.ac.jp (Y.S.); nguele@mine.kyushu-u.ac.jp (R.N.)

[2] Institute for Future Engineering (IFENG), Tokyo 135-8473, Japan

* Correspondence: sreu.tola@mine.kyushu-u.ac.jp

Abstract: The underlying effect of preflush salinity and silica nanofluid (Si-NF) on oil production is examined. The influence of salinity on the stability of Si-NFs is studied. A series of sand-pack floodings evaluating oil production was conducted at different concentrations of preflush salinity (0 to 4 wt.%), followed by the injection of a Si-NF (0.5 wt.%) at the trail of which postflush water was injected. The effluent water and solids were collected and analyzed using X-ray fluorescence (XRF). Interfacial tension (IFT) and contact angle measurements were conducted on the Si-NF in the presence of salinity to confirm the effect. The Si-NF became unstable and formed precipitate in the presence of salinity. The sand-pack flooding showed that when the preflush salinity was increased, the displacement efficiency (E_D) using the Si-NF and postflush injection was increased ($E_D = 44\%$). The XRF of the precipitated effluent revealed that the preflush salinity and Si-NF caused mineral leaching, which triggered pore clogging. The IFT value reduced from 13.3 to 8.2 mN/m, and the wettability was altered to be more strongly water-wet when the salinity increased. The primary mechanisms of oil recovery using the Si-NF after preflush salinity is attributed mainly to the clogging mechanism. This clogging helps block the high-perm area, shift the fluid flow to the oil-trapped zone, and free the oil out. Other contribution mechanisms are IFT reduction and wettability alteration.

Keywords: enhanced oil recovery; sand-pack flooding; silica nanofluid; precipitation; sedimentation; saline water; pore clogging; interfacial tension; contact angle; wettability alteration

1. Introduction

Up to 75% of oil in place remains underground at the end of primary and secondary oil production, with a significant portion trapped within the narrow pore throats. This is because the capillary forces which keep the oil droplets attached to the rock surface are so strong that neither the natural energy of the oil-bearing matrix (primary production) nor the injection of water and/or gas (secondary production) can overcome them. These capillary forces are subsequent to the interactions between the surface charges of the formation rock and the polar groups of the stranded oil [1].

At this stage, the increment in oil production—also termed as enhanced oil recovery, or EOR—results from the injection of foreign fluids, energy (i.e., heat) or the combination of both. This prompts several oil production mechanisms, including (1) a reduction in interfacial tension, or IFT, between the stranded fluids [2–6], (2) oil swelling [7–9], (3) a reduction in oil viscosity [10–12], or (4) a wettability alteration from oil-wet to water-wet [1,13,14].

The literature argues that nanoparticles (NPs) could overcome the challenges associated with conventional EOR methods, while increasing the oil production. For example, alkaline, surfactant, and polymer floodings are known to increase the additional oil production to up to 20% [15–17]. However, these techniques suffer from chemical loss due to adsorption onto the formation matrix [18–21]. Y. Wu et al. [22] found that adding silica

NPs at the concentration of 0.2 wt.% could lower the chemical loss (surfactant adsorption on rock) from 1.16 to 0.77 mg/g. At the same time, silica NP–surfactant flooding improves the oil production efficiency by 4.68% higher than normal surfactant flooding.

As far as nanoparticle-EOR is concerned, silica oxide nanoparticles (Si-NP) are one of the most prominent materials as evidenced by the wealth in literature [22–28]. Sharma and Sangwai [26] studied the potential of a silica oxide nanofluid (Si-NF) formulated by dispersing Si-NPs into polyacrylamide with and without a surfactant. The authors claimed that that the presence of the Si-NF reduces the IFT on both the polymer and surfactant. Ogolo et al. [29] argued that Si-NPs dispersed in ethanol improved oil recovery through the change of rock wettability. Hendraningrat et al. [30] studied the transport of hydrophilic Si-NPs in a glass micromodel experiment. They observed that NPs caused pore-blockage and deposition, which triggered the permeability impairment in porous media.

Based on the available literature, it appears that the primary mechanisms associated with oil production using Si-NF include, primarily, (1) IFT reduction [14,31,32], (2) wettability alteration [14,33–35], (3) the prevention of asphaltene precipitation [36,37], and (4) porosity impairment [30,38,39]. However, most of the published works fail to address the contribution of the formation salinity.

In reality, prior to Si-NF injection, the formation is preflushed with water, usually with low saline water (Figure 1a).
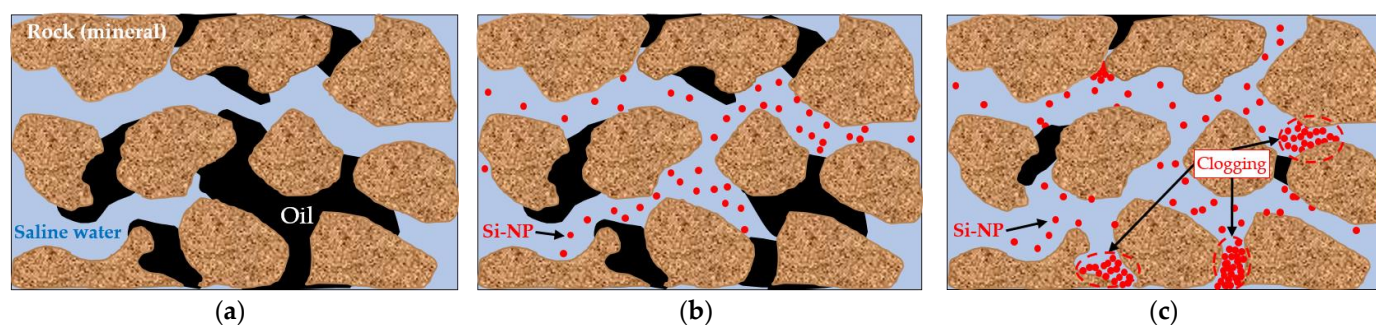

(a)　　　　　　　　　　　　　　　　(b)　　　　　　　　　　　　　　　　(c)

Figure 1. Plausible clogging mechanism of Si-NF in porous media in the presence of saline water (flow direction from left to right). (**a**) Preflushed formation; (**b**) injection of Si-NF; (**c**) after injection of Si-NF.

The preflush is designed to displace away from the wellbore formation brines that contain several ions, including potassium, sodium, and calcium [1,40,41]. In doing so, the crystallization of alkali-fluosilicates is lowered and formation damage is mitigated. As the Si-NF propagates in the formation water (Figure 1b), it dilutes with the resident water, which breaks the stability of the Si-NF due to reducing the repulsion forces of the Si-NPs [42]. The unstable Si-NF then precipitates and clogs the pore throats, which causes the pathway of the injectant to divert.

The injectant can then flow to push trapped oil from the unswept zone (Figure 1c). As such, the instability of Si-NPs in a saline environment is one of the challenges of EOR [43]. This is to state that there are still some unclarified questions that, if answered, could improve the potential of NFs. These include, for example, the interactions with the formation rock, crude oil/brine/rock (COBR), in addition to the interaction of the Si-NF in the saline environment that might be linked to the change of the Si-NF's surface chemistry.

The change of the Si-NF's surface chemistry might cause a liquid–liquid interaction (IFT between Si-NF and crude oil), liquid–solid interaction (Si-NF and porous media in wettability alteration), and pore blockage due to an instability of the Si-NF in the pore throat.

Therefore, the present work investigates the contribution of the preflush salinity on the stability of the Si-NF and its implication to oil recovery. To achieve the objective, we conduct a series of sand-pack flooding experiments with different preflush salinity concentrations, followed by a Si-NF and postflush injection to evaluate the displacement efficiency. Furthermore, the chemistry of the effluent water is examined using spectral

analyses. Finally, both the wettability and the IFT measurements were carried out to study the effect of salinity in the Si-NF.

2. Materials and Methods

2.1. Materials

2.1.1. Nanoparticles

Silica oxide nanoparticles (Si-NPs) were selected as the primary material to prepare the nanofluid. Si-NPs were purchased from Tecnan (Tecnan, Las Acros, Spain). As per the supplier, Si-NPs were a 99.9% pure white powder with a particle size ranging from 10 to 15 nm and a surface area ranging from 152 to 229 m^2/g.

2.1.2. Reservoir Fluid

The formation water (FW) was prepared in-house from sodium chloride (NaCl), purchased from Junsei Chemical (Junsei Chemical, Tokyo, Japan); FW consists of 4 wt.% NaCl. The candidate oil was a light Japanese crude oil (hereinafter LJO) sampled from a Japanese oilfield with a density of 0.860 g/cm^3 and a viscosity of 9.54 cP. Both the density and the viscosity of the candidate oil were measured at room temperature. Additionally, LJO had an acidity number of 1.86 mg-KOH/g-oil measured as per ASTM D664 [44].

2.1.3. Porous Media

Grinded Berea sandstone, with a particle size ranging from 60 to around 180 μm, modeled the formation rock, whose properties are outlined in Table 1.

Table 1. Elemental composition of the model rock (in wt.%).

Silicon (Si)	Aluminum (Al)	Calcium (Ca)	Potassium (K)	Sodium (Na)	Magnesium (Mg)	Iron (Fe)	Titanium (Ti)
71.7	8.07	5.73	8.44	0.62	0.13	3.51	1.21

2.2. Methods

2.2.1. Preflush Water Composition

Four water compositions were prepared by dissolving NaCl in deionized water. They were used for preflush and postflush. The viscosity was measured using a rotational spindle rotor (Brookfield, model DV1), and the density was measure using a pycnometer. The physico-chemical properties of preflush water are listed in Table 2.

Table 2. Physico-chemical properties of preflush water used in this study [a].

Code	Salinity (wt.% NaCl)	μ (cP)	ρ (g/cm^3)
P-1 (deionized water)	-	1.0~1.5	0.997 ± 0.002
P-2	0.50	1.0~1.5	1.000 ± 0.002
P-3	2.00	1.0~1.5	1.011 ± 0.002
P-4 (FW)	4.00	1.0~1.5	1.025 ± 0.002

[a] μ: viscosity; ρ: density.

2.2.2. Nanofluid Preparation and Stability in Saline Environment

Si-NF was prepared by mixing 0.5 g of Si-NPs into 100 g of deionized water and was sonicated using an ultrasonic bath (AS ONE US = 3R) for 70 min. Cold water was cycled in the ultrasonic bath during the sonicating stage to maintain temperature rise subsequent to ultrasonic vibration [45].

To investigate Si-NF's stability in a saline environment, we dissolved NaCl at different mass concentrations into a prepared Si-NF and monitored its stability for seven days. To do so, a sedimentation technique was used to evaluate the sedimentation mass of Si-NP [46].

First, a known mass of Si-NF supernatant ($mass_{before\ dry}$) was taken out from a Si-NF stock solution each day for seven days.

Each supernatant was then dried in the oven at 105 °C for 24 h. Finally, the dry supernatant ($mass_{after\ dry}$) was weighed again and was calculated for a weight percent of sedimentation (wt.% sedimentation) using this formula:

$$wt.\%\ sedimentation = wt.\%\ stock\ solution - wt.\%\ supernatant$$

where

$$wt.\%\ stock\ solution = wt.\%\ Si\text{-}NF + wt.\%\ NaCl$$

and

$$wt.\%\ supernatant = (mass_{after\ dry}/mass_{before\ dry}) \times 100$$

The zeta-potential and dynamic light scattering (DLS) of Si-NF under saline environment were also characterized using ELS-800 (Otsuka Electronics, Osaka, Japan), whose measurement principle is based on electrophoresis light scattering method using He–Ne laser as the light source. The zeta-potential is the measurement of electric potential, and it is significant because its value can be linked to the stability of colloidal dispersions. Colloids with a high zeta-potential (negative or positive) are electrically stable, whereas those with a low zeta-potential coagulate or flocculate [46–49].

2.2.3. Interfacial Tension and Contact Angle Measurements

Interfacial tension (IFT) and contact angle measurements were performed at ambient conditions on an apparatus DropMaster DMs-401 (Kyowa Interface Science Co., Ltd., Tokyo, Japan) schematized in Figure 2.
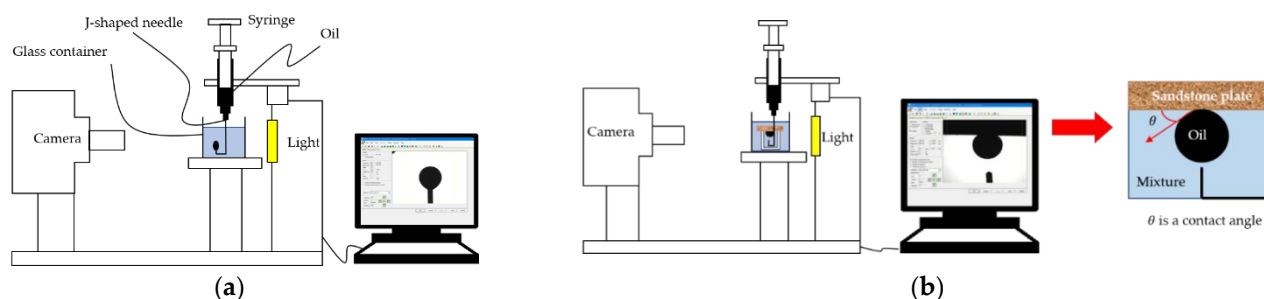

(a)   **(b)**

Figure 2. Schematic of IFT and contact angle measurement. Reprinted with permission from Nguele et al. [28], © (2019) American Chemical Society. (**a**) IFT measurement set up; (**b**) contact angle measurement set up.

An oil droplet (~5 μL) was released from a J-shaped needle into a glass container priorly filled with Si-NF and saline water. The camera then captured the oil droplet, and the image was processed automatically by an in-built software (Figure 2a). The wettability of the sandstone, on the other hand, was evaluated by contact angle measurement using the sessile drop method (Figure 2b).

Prior to the measurements, the sandstone plates were cut from the Berea sandstone core into small pieces with a length of 1.5 cm, a width of 1.5 cm, and a thickness of 0.5 cm. The sandstone plate was then saturated with LJO and aged for a week at 70 °C to ensure a complete oil-wet surface [50]. Then, the oil-saturated sandstone plate was placed horizontally into the glass containing Si-NF and saline water.

The oil droplet was then released from a J-shaped needle below the rock segment and was allowed to stick on that surface for about 5 min. The image's shape was captured and processed using an in-build software, and the contact angle was recorded. The control experiments consisted in measuring the contact angle on an oil-free sandstone plate.

2.2.4. Sand-Pack Flooding Experiments

A designed sand-pack (SP) system with a length of 10 cm and a diameter of 2.50 cm created from a transparent acrylic tube was prepared (Figure 3).
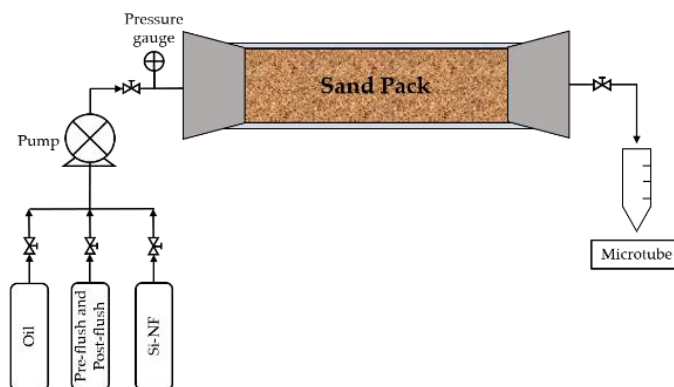

Figure 3. Schematic of sand-pack flooding experiment used in this study.

The porous filters (diameter of 40 μm) were placed both at the inlet and outlet of the sand-pack to prevent sand particles from blocking the tube line. The oil recovery was commenced by the injection formation water (i.e., 4 wt.% NaCl) for about 3 pore volumes (PV) at the trail of which crude oil was injected in the sand-pack until no more water was produced from the outlet. The sand-pack was then aged overnight.

The preflush was injected until the water cut reached around 98~99%. Si-NF was then injected for 1 PV and followed by 2 PV drive water, whose salinity was equal to that of the preflush water. The pressure drop across the sand-pack was recorded using a pressure gauge installed at the inlet. The effluent fluids were collected and were stored in a microtube. It is worth mentioning that all the floodings were conducted at ambient conditions and the same flow rate of 0.5 cc/min.

3. Results and Discussions

3.1. Stability of Nanofluid in Saline Environment

3.1.1. Sedimentation Test

Figure 4 showed that all of the Si-NF seemed stable in the first 24 h. However, the Si-NF started to precipitate from day 2, and the amount of sedimentation reached the maximum on day 3.
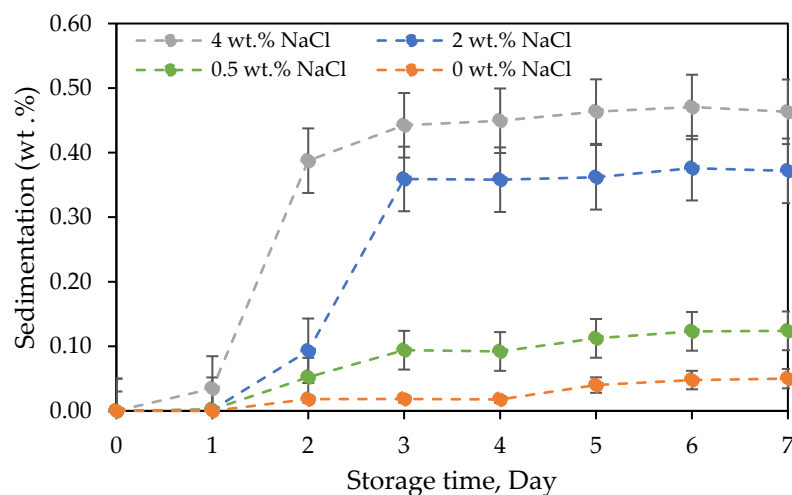

Figure 4. Effect of NaCl concentration on sedimentation.

It was also noticed that the amount of NaCl caused the increase in sedimentation in the Si-NF. For example, when 4 wt.% of NaCl was added to the Si-NF, the sedimentation was as high as 0.47 wt.%, which was almost equal to the amount of Si-NF (0.5 wt.%).

The sedimentation volume can be observed visually in Figure 5. It is clear that the Si-NF prepared without NaCl (deionized water) was more stable without any visible sedimentation. Moreover, the sedimentation volume increased when NaCl increased. The sedimentation of the Si-NF in the presence of NaCl appeared such as a gel sediment.

Figure 5. Picture of Si-NF at different NaCl concentrations (0, 0.5, 2, and 4 wt.% from left to right) at day 7.

3.1.2. Zeta-Potential and Particles Size Distribution

Figure 6 shows the value of the zeta-potential and pH change of the Si-NF in NaCl. The absolute zeta-potential of the original Si-NF (0 wt.% NaCl) was 25.31 mV, indicating a moderately stable fluid as per the literature [48,49]. However, when NaCl was added to the Si-NF, the absolute zeta-potential decreased and kept decreasing to 4.41 mV. This significant decrease in zeta-potential indicated that the Si-NF lost its repulsion force leading to destabilization.
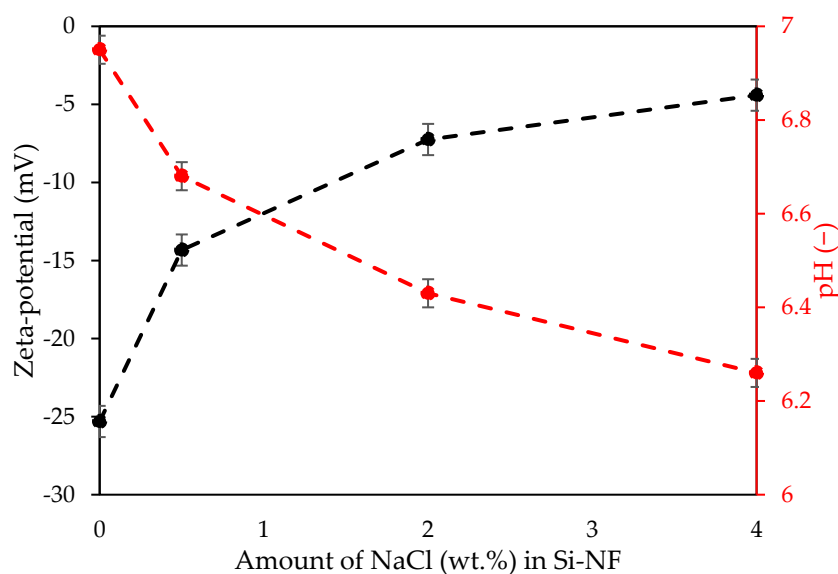

Figure 6. Effect of NaCl concentration on zeta-potential and pH.

Looking at the pH in the same figure, we also noticed that the pH decreased when NaCl increased. The pH is contributed to the Si-NF stability [51–54]. Qu and Wu [55] prepared SiO_2–water nanofluids, and they adjusted the pH value of the water to 9.7, which

was far away from the isoelectric point (IEP) of silica (pH~3), and then nanoparticles (0.1 to 0.5 wt.%) were added into that water and, subsequently, vibrated for about 4 hrs in an ultrasonic bath; their technique allowed the nanofluid to become stable for several days. It is recommended that the pH of a stable nanofluid should be kept away from IEP in order to increase the surface charge of the nanoparticles due to the more frequent attachment of surface hydroxyl groups [56].

Figure 7 shows the DLS analysis of the Si-NF particle size distribution in the presence of NaCl. The Si-NF had a small particle size distribution at 0 wt.% NaCl; this indicated a better dispersion of Si-NF. However, the particles size distribution increased more when NaCl increased. The increase in the particles size distribution resulted from the aggregation of unstable Si-NF with NaCl.
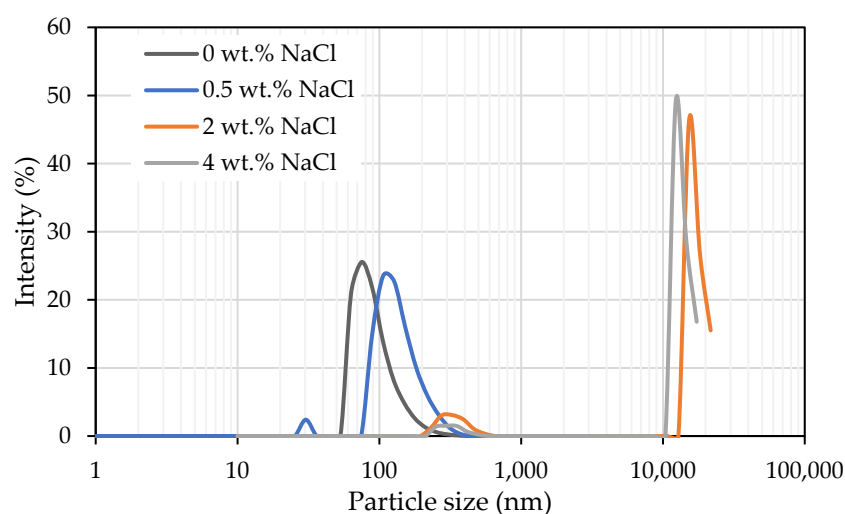

Figure 7. Effect of NaCl concentration on the particles size distribution.

This study found that NaCl reduced both the pH and absolute zeta-potential of Si-NF or decreased the surface charge, so when the surface charge reduced, it reduced the repulsion force between the particles in the colloid. In other words, NaCl caused the Si-NF to precipitate.

3.2. Effect of IFT and Wettability on Nanofluid in Saline Environment

3.2.1. IFT Reduction

It is well established that IFT is a critical element in EOR processes because it influences capillary forces, which are responsible for mobilizing trapped oil [57–59]. Figure 8 shows that the IFT of the original Si-NF (0 wt.% NaCl) was 13.3 mN/m; it reduced from 13.3 to 8.2 mN/m when increasing the salinity concentration.

A similar IFT reduction in the salinity effect was also observed by H. Farhadi et al. [60]. Aside from destabilizing the Si-NF, it showed that NaCl in Si-NF could help reduce IFT. According to the Gibbs adsorption isotherm, the presence of salt (NaCl) at the interface lowers IFT by making the surface excess concentration (Γ) positive [50]. However, IFT reached its lowest value after 2 wt.% NaCl was added, which is suggested to be the salting-out effect [61].

3.2.2. Wettability Alteration

Figure 9 shows the contact angle of an oil droplet spreading on the sandstone plate. In the control experiment (oil-free sandstone plate), we found a minor change in the contact angle when salt was added into the Si-NF. The contact angle (θ) was between 38.5° and 34.3°, indicating the water-wet condition as per the literature [1,62].
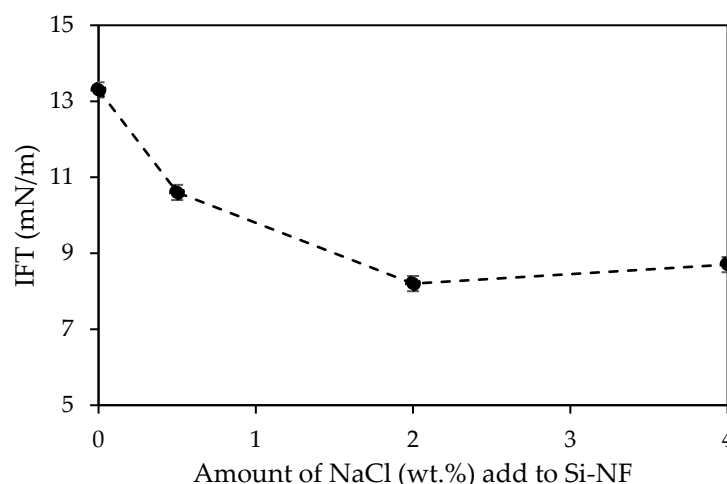
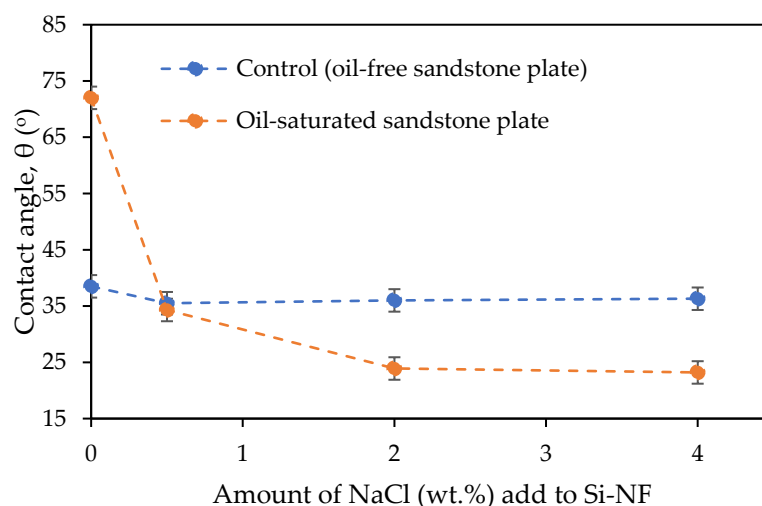**Figure 8.** Effect of NaCl concentration on IFT.

Figure 9. Effect of NaCl concentration on contact angle between oil droplet and sandstone plate.

However, in the oil-saturated sandstone plate, we saw that the contact angle without NaCl was high ($\theta = 72°$) and kept decreasing when NaCl was added and reduced to $\theta = 23.2°$. The decrease in the contact angle in the oil-saturated sandstone plate when NaCl increased was believed to be due to the diffusion of NaCl on the oil-film layer of the oil-saturated sandstone plate. NaCl diffusion was, seemly, activating the Si-NF to form a self-assembled wedge-shaped film in contact with the oil phase. The wedge film, then, separated the oil droplets from the rock surface. The wedge-shaped film was formed due to a pressure known as structural disjoining pressure [63–65].

While in the control experiment, the Si-NF, seemly, formed a wedge film on the water-film layer and created disjoining pressure on the oil droplet, resulting in a low contact angle value without NaCl. Therefore, adding NaCl to the Si-NF in an oil-free sandstone plate was less effective in reducing the contact angle. However, at a high concentration (above 2 wt.% NaCl), the contact angle did not improve anymore as opposed to the trend shown by the IFT (Figure 8).

3.3. Oil Recovery by Sand-Pack Flooding

To evaluate the potential of the Si-NF in displacing the candidate light oil, we conducted a series of eight sand-pack flooding experiments at room temperature, i.e., 25 °C.

The oil production was divided into three parts: (1) the preflush, (2) Si-NF flooding, and (3) postflush. During the preflush, four different salinity concentrations were used,

including 0, 0.5, 2, and 4 wt.% NaCl. After that, the Si-NF was injected and followed by the postflush injection.

Looking at the displacement efficiency (E_D), as shown in Table 3, it can be observed that the preflush affected the increment of the EOR. The details on oil production were discussed in the following Sections regarding the effect of the preflush salinity and formation rock mineralogy.

Table 3. Summary on oil recovery using sand-pack flooding at 0.5% Si-NF [b].

Run	Porous Media	L (cm)	D (cm)	PV (mL)	Φ (%)	S_o (−)	Preflush (NaCl)		Si-NF 0.5 wt.%	Postflush (NaCl)		E_D (%)
							C (wt.%)	S_{o1} (−)	S_{o2} (−)	C (wt.%)	S_{o3} (−)	
SP-1		8.75	2.50	17.9	41.7	0.77	0	0.135	0.135	0	0.135	0.00
SP-2	Grinded	8.75	2.50	18.3	42.6	0.77	0.5	0.164	0.143	0.5	0.135	17.56
SP-3	sandstone	8.65	2.50	17.7	41.6	0.75	2	0.228	0.142	2	0.138	39.16
SP-4		8.45	2.50	17.0	41.1	0.74	4	0.227	0.144	4	0.127	43.93
SP-5		8.85	2.50	16.3	37.5	0.89	0	0.323	0.299	0	0.270	16.30
SP-6	Glass	8.98	2.50	16.7	37.8	0.88	0.5	0.307	0.286	0.5	0.248	19.40
SP-7	bead	8.90	2.50	16.5	37.8	0.88	2	0.357	0.345	2	0.314	11.98
SP-8		8.96	2.50	16.7	37.9	0.89	4	0.345	0.329	4	0.265	23.04

[b] *L*: length; *D*: diameter; *PV*: pore volume; Φ: porosity; S_o: oil saturation; *C*: concentration; E_D: displacement efficiency $E_D = 100 * (1 − (S_{o3}/S_{o1}))$.

3.3.1. Effect of Preflush Salinity

The control experiment (SP-1) consisted of an injection preflush salinity of 0 wt.% NaCl (deionized water). The results are shown in Figure 10a. It was found that the preflush yielded an oil recovery of 82%. However, no additional oil was observed when the Si-NF and postflush were injected, as no increase in the displacement efficiency was recorded ($E_D = 0$).

Then, the increase in preflush salinity was performed in SP-2, SP-3, and SP-4 (Figure 10b–d), respectively, to the increase in the preflush salinity concentration of 0.5, 2, and 4 wt.% NaCl. As a result, we found that the oil recovery during the preflush was different from the control experiment. It appeared that the oil recovery during the preflush stage decreased to 78, 70, and 69%, respectively, to the increase in the preflush salinity concentration of 0.5, 2, and 4 wt.% NaCl. These results explained that the preflush salinity in the preflush stage affected the oil recovery. The mechanism of the salinity effect was described by others in their published works [4,66,67]. For this study, we focused mainly on the displacement efficiency when the Si-NF was used after that preflush salinity. Interestingly, we found that SP-2, SP-3, and SP-4 increased the displacement efficiency (E_D = 17.56, 39.16 and 43.93%), respectively, after the Si-NF was used (Figure 10b–d).

The increment in oil during Si-NF injection was concurrent with an increase in the pressure drop. The pressure drop increased during Si-NF injection as a function of preflush salinity—the higher the preflush salinity concentration, the higher the pressure drop increase—and it is believed to have happened due to the instability of the Si-NF in a saline environment.
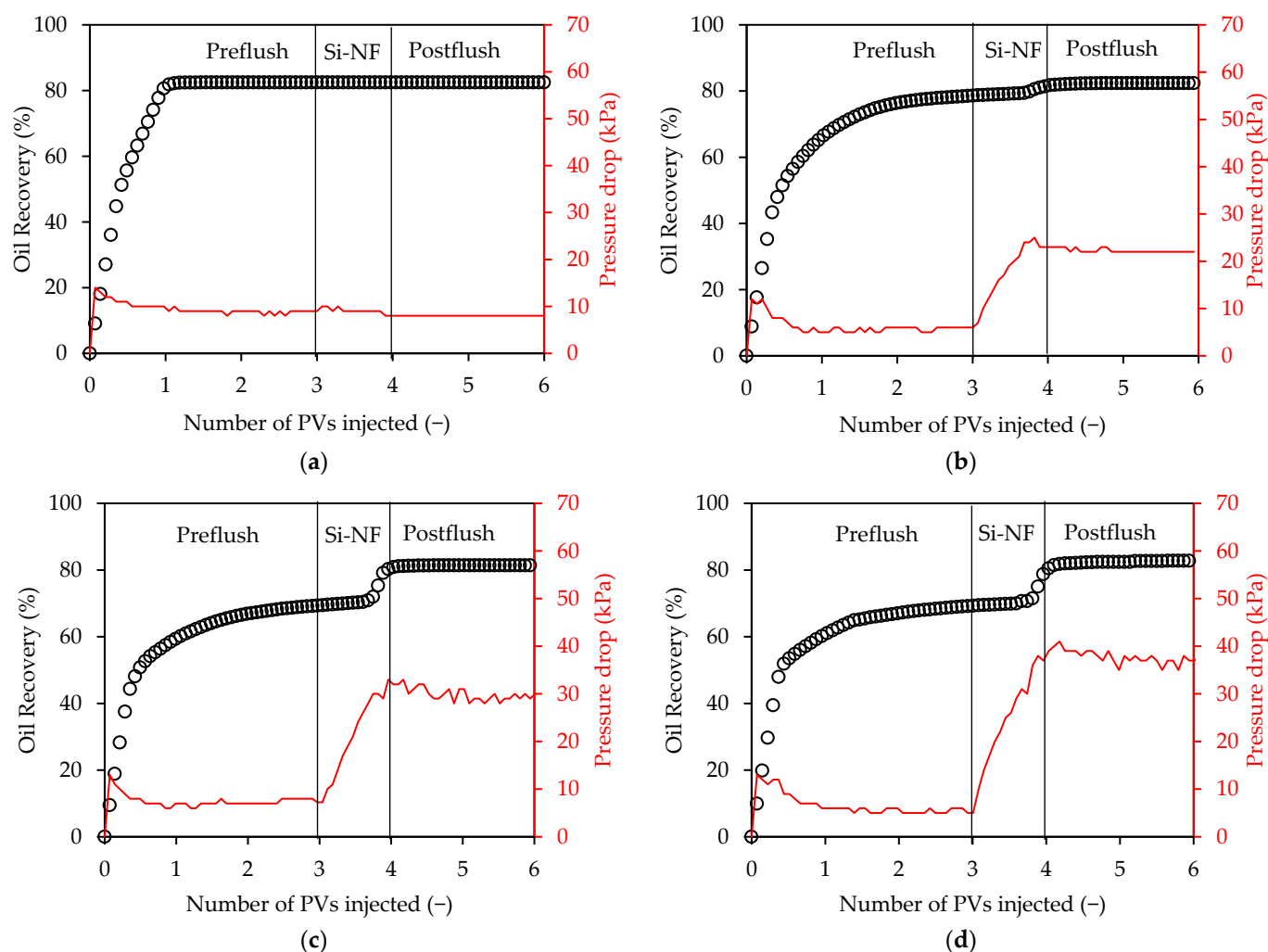
Figure 10. Effect of preflush salinity on oil recovery. (**a**) Control experiment, 0 wt.% (SP-1); (**b**) 0.5 wt.% (SP-2); (**c**) 2 wt.% (SP-3); (**d**) 4 wt.% (SP-4).

3.3.2. Effect of Formation Rock Mineralogy

During the sand-pack flooding experiment, we observed a change in the effluent water. The effluent water was found to form a precipitate during the Si-NF stage (SP-2, SP-3, and SP-4), as shown in Figure 11b–d. At the same time, no precipitate was observed when the Si-NF was used in SP-1 (Figure 11a). Our most intriguing observation was that the precipitate in the effluent water linked to the presence of salinity in the preflush. As we can see in Figure 11a, the preflush had 0 wt.% NaCl and no precipitate occurred, which can be explained by NaCl in the preflush causing the Si-NF to precipitate, which was reported in the stability of the nanofluid Section above.

Moreover, there were some small frictions of oil deposition found mainly in the effluent water during the preflush. However, less or no oil deposition was observed in effluents during the Si-NF and postflush injection. This can be explained because of the Si-NPs. The absorption of Si-NPs on the surface of asphaltene molecules significantly reduced the asphaltene precipitation [36,64,68,69]; in order words, this reduced the oil deposition.

To evaluate the precipitate, we took the effluent from SP-2, SP-3, and SP-4, then dried it out to conduct spectral analyses. As shown in Figure 12, the dry effluents' chemical composition was analyzed using the XRF technique (XRF, ZSX Primus II, Rigaku Corporation, Tokyo, Japan).
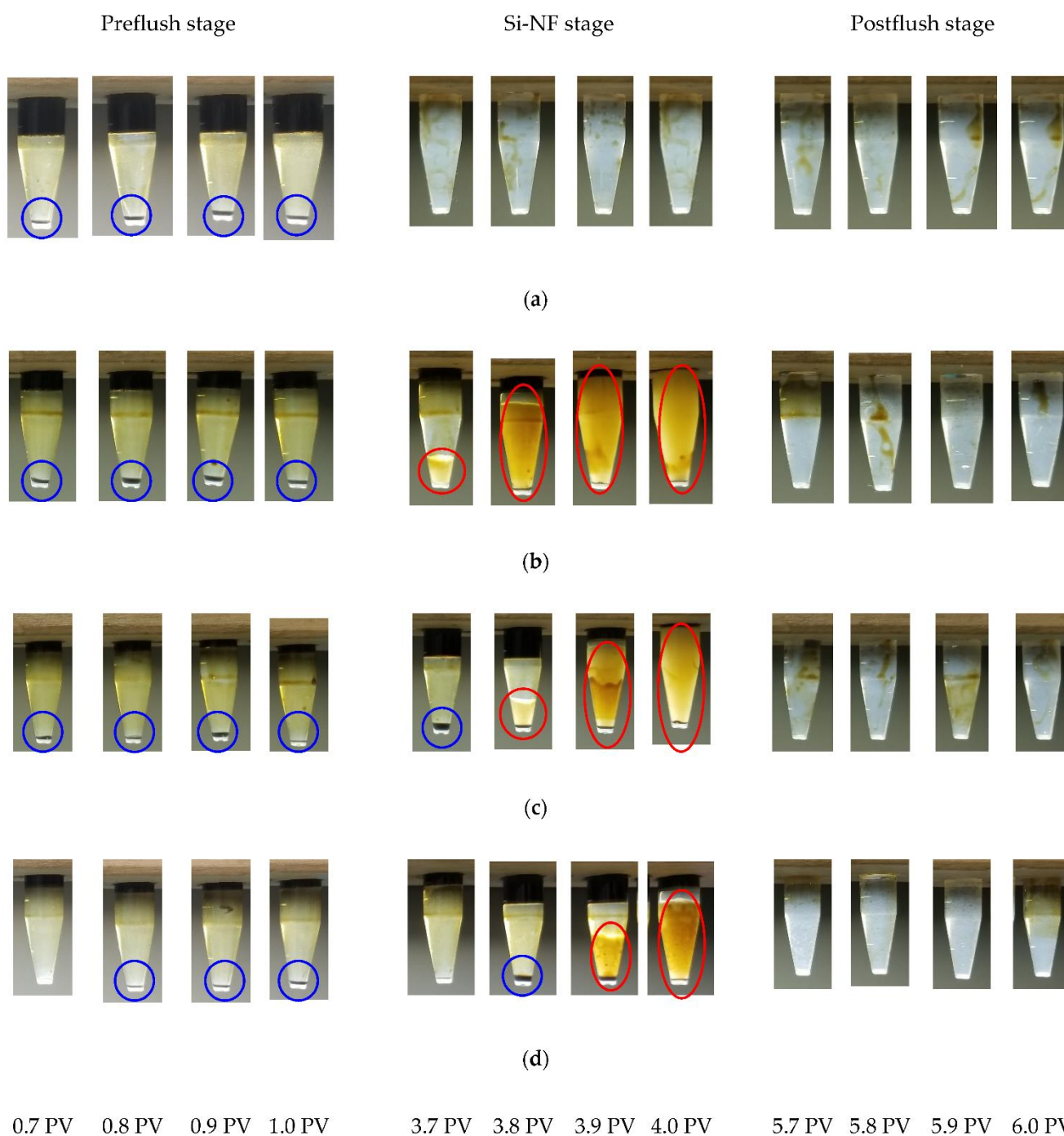
Preflush stage　　　　　　　Si-NF stage　　　　　　　Postflush stage

(a)

(b)

(c)

(d)

0.7 PV　0.8 PV　0.9 PV　1.0 PV　　3.7 PV　3.8 PV　3.9 PV　4.0 PV　　5.7 PV　5.8 PV　5.9 PV　6.0 PV

Figure 11. Picture of effluents during preflush, Si-NF, and postflush at specific pore volume injections; the circle in blue shows oil deposition, that in red shows precipitation. (**a**) Control experiment, 0 wt.% NaCl (SP-1); (**b**) 0.50 wt.% NaCl (SP-2); (**c**) 2.00 wt.% NaCl (SP-3); (**d**) 4.00 wt.% NaCl (SP-4).

By comparing to the dry Si-NF, we found that most of the precipitate consisted of silicon (Si), aluminum (Al), and potassium (K), which were similar to the modeled rock's chemical composition. These results suggested that the precipitate came from the Si-NF and came from porous media leaching. The leaching may have come from alkali feldspars' minerals, including potassium aluminosilicate ($KAlSi_3O_8$) or/and sodium aluminosilicate ($NaAlSi_3O_8$).
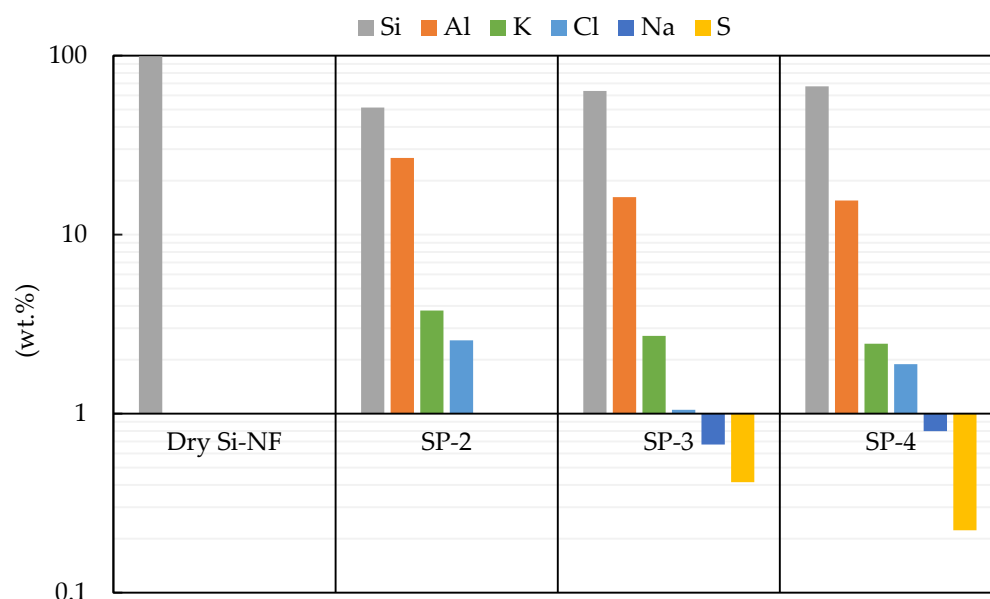
Figure 12. Chemical compositions of precipitated effluent during Si-NF injection.

In addition, the presence of sodium (Na) and chloride (Cl) was the result of the preflush salinity that composed the NaCl. However, the amount of Na could not be detected in SP-2, which was probably due to the small amount of preflush salinity (0.5 wt.% NaCl) and Na dissolution during Si-NF injection. It is also possible that the precipitate was caused by the binding of segregated Si-NP with trapped oil, where a tiny amount of sulfide (S) was found in the effluent of SP-3 and SP-4.

It is believed that the precipitate in effluent water led to an increase in E_D due to the pore channel clogging effect. It was explained that Si-NPs accumulated and caused a pore throat blockage, which caused pressure to build up in the adjacent pore throat, forcing the oil trapped in the pore throat out. When the oil is released, the surrounding pressure lowers, the clogging gradually dissipates, and the Si-NPs begin to flow with the water; this is referred to as log-jamming [64].

On the other hand, some studies confirm that the clogging phenomena may cause a permeability and porosity impairment, which is unfavorable for oil production [70,71]. Conversely, the clogging mechanism of Si-NF injection seemed to cause a temporary blockage rather than a permanent one that ruins the oil production. A study on the flow of nano-dispersed catalyst particles through porous media revealed that, at a lower permeability, an increased operating temperature, and a higher particle concentration, the propagation of the nano-dispersed catalyst suspension through the media was not significantly affected [72].

However, there was no clear evidence to state whether an unstable Si-NF or mineral leaching caused clogging that primarily contributed to the E_D. One can state that the unstable Si-NF is the primarily clogging mechanism, unless rock mineralogy is neglected. For this purpose, we conducted another sand-pack flooding experiment using glass beads. A glass bead is a non-reactive media, which eliminated the contribution of the rock mineralogy in this study. Its particle size ranged from 105 to 125 μm.

In glass beads, we injected 4 PV of preflush and 1 PV of Si-NF, following by 2 PV of postflush (Figure 13a–d). As a result, the oil recovery of glass beads during preflush was between 59 and 62%. The E_D of glass beads was between 11.9 and 23%. Additionally, we observed that the pressure drop increased when the Si-NF was used, and the higher the salinity in the preflush, the higher was the pressure drop in the Si-NF stage.
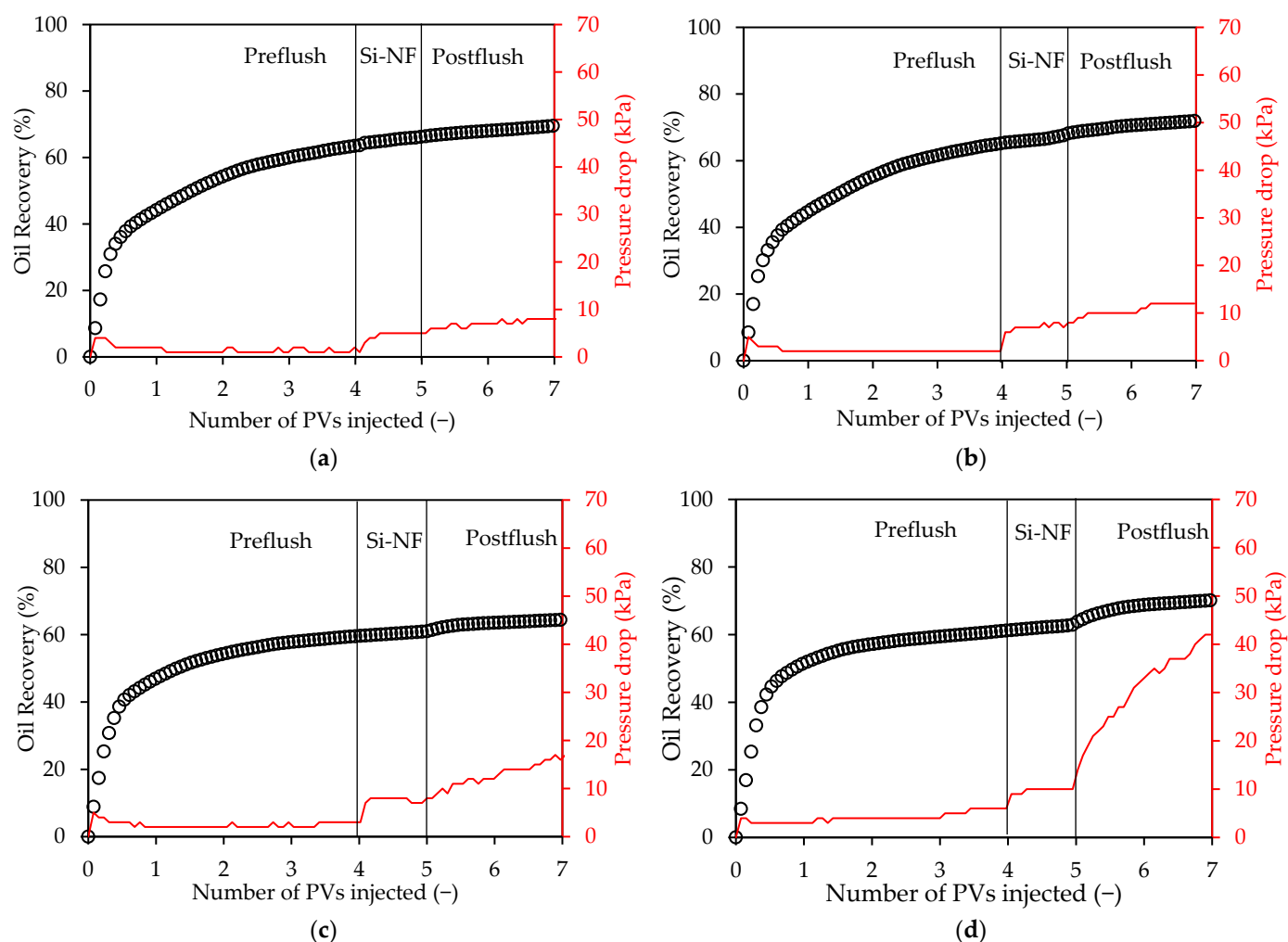
Figure 13. Effect of preflush salinity in glass beads. (**a**) Control experiment, 0 wt.% NaCl (SP-5); (**b**) 0.5 wt.% NaCl (SP-6); (**c**) 2 wt.% NaCl (SP-7); (**d**) 4 wt.% NaCl (SP-8).

When comparing the displacement efficiency of glass beads and grinded Berea sandstone at the same preflush salinity of 4 wt.% NaCl, we realized that grinded Berea sandstone yielded a higher displacement efficiency than the glass beads case (E_D = 43.93% and 23.04%), respectively. More importantly, we did not observe any precipitate from all cases of sandpack flooding in glass beads. For this reason, we believed that the interactions of formation rock mineralogy and Si-NF contributed to the higher displacement efficiency, for example, in the grinded Berea sandstone case.

We understood from the series of experiments using glass beads that Si-NF could still clog the media, since an increasing pressure drop was observed. Hence, the Si-NF was the main primary factor that caused clogging in the media.

Figure 14 shows the top view photos of two different sand-pack scenarios. It could be seen that the less-oil area (red enclosed line) appeared during the preflush in grinded Berea sandstone (Figure 14a). During Si-NF injection, we could observe that the less-oil area expanded, and the proportion of the oil bank was pushed to the outlet; this oil bank provided more oil production during Si-NF flooding. At the end of the postflush, we observed that the less-oil area was completely saturated, meaning that most of the oil trapped was produced.
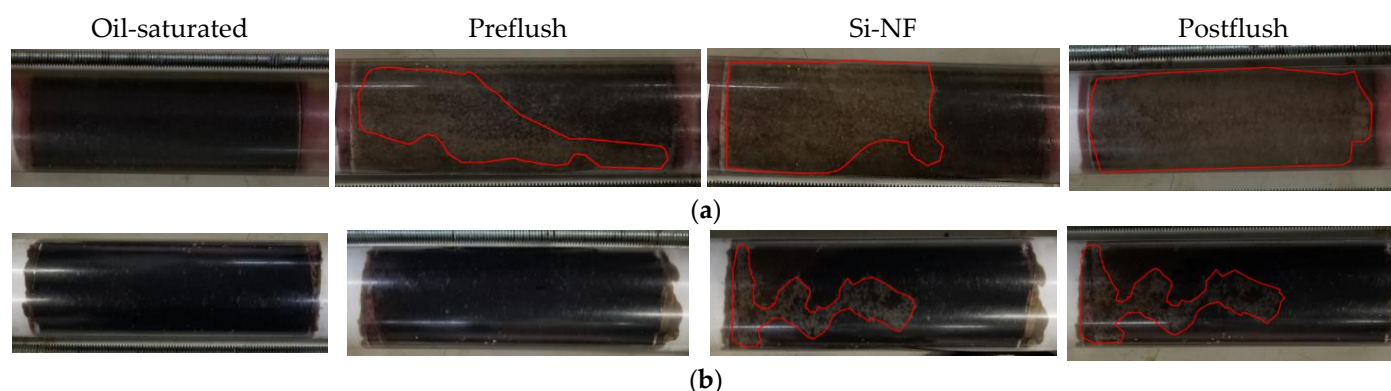
Oil-saturated	Preflush	Si-NF	Postflush

(**a**)

(**b**)

Figure 14. Top view photos of sand-pack during flooding, injection from left to right (red enclosed line is less-oil area). (**a**) Grinded Berea sandstone (preflush = 4 wt.% NaCl); (**b**) glass beads (preflush = 4 wt.% NaCl).

Dissimilar to the grinded Berea sandstone, the glass beads did not form a clear less-oil area during the preflush. However, when the Si-NF was injected, it created a different flow pattern of the less-oil area from the grinded Berea sandstone case, and the flow pattern was slightly increased in the postflush (Figure 14b). It could be explained that the Si-NF propagation caused these flow patterns in both media, which diverted the injectant to an unswept oil-trapped zone and pushed more oil out.

The pore channel clogging effect in this study was caused by the instability of the Si-NF in a saline environment triggered by the interactions between Si-NF with NaCl; this interaction could trigger the particle size of the injectant to expand, and by enlarging the diameter, it would act as a barrier to clog the pore throat, especially the high-permeability area, which is why the pressure drop increased when the Si-NF was injected.

4. Conclusions

The main conclusions herein were drawn together and demonstrate the influence of the preflush salinity and Si-NF in oil production. The key findings were as follows:

- Salinity caused an instability to the Si-NF due to the decrease in the absolute zeta-potential value (25.31 to 4.41 mV), which triggered the reduction in repulsion force on the Si-NF. In addition, the particles size distribution of the Si-NF also increased due to the aggregation of Si-NF and NaCl.
- Increasing NaCl in the Si-NF caused an IFT reduction (from 13.3 to 8.2 mN/m) and wettability alteration to strongly water-wet conditions (from 72 to 23.2°).
- The XRF results of the precipitated effluent revealed that the precipitation was formed from the unstable Si-NF and the mineral leaching in the porous media.
- A displacement efficiency of up to 44% could be achieved by increasing the preflush salinity; then, injecting the Si-NF and the postflush.

This study showed that the increasing preflush salinity impacted oil recovery when the Si-NF and postflush were employed. The dominant mechanism of oil production using the Si-NF was due to the clogging effect; this clogging helped to block the high-permeability area and divert the fluid flow to the oil-trapped zone and force the oil out. Other contributions to the oil production were due to the IFT reduction and wettability alteration in the presence of the Si-NF and saline environment. Some improvements, such as reservoir pressure and temperature during flooding experiments, could be implemented in future investigations.

References

1. Donaldson, E.C.; Alam, W. *Wettability*; Gulf Pub. Co.: Houston, TX, USA, 2008; ISBN 9781933762296.
2. Martyushev, D.A.; Vinogradov, J. Development and application of a double action acidic emulsion for improved oil well performance: Laboratory tests and field trials. *Colloids Surf. A Physicochem. Eng. Asp.* **2021**, *612*, 125998. [CrossRef]
3. Sugai, Y.; Komatsu, K.; Sasaki, K. Estimation of IFT reduction by a biomass material and potential of its utilization for EOR. In Proceedings of the SPE/IATMI Asia Pacific Oil & Gas Conference and Exhibition, Nusa Dua, Bali, Indonesia, 22–25 October 2015.
4. Mohammad Salehi, M.; Omidvar, P.; Naeimi, F. Salinity of injection water and its impact on oil recovery absolute permeability, residual oil saturation, interfacial tension and capillary pressure. *Egypt. J. Pet.* **2017**, *26*, 301–312. [CrossRef]
5. Shagiakhmetov, A.M.; Tananykhin, D.S.; Martyushev, D.A.; Lekomtsev, A.V. Investigation of the temperature influence on the gelation and the strength of water-shutoff composition based on carboxymethyl cellulose. *Neft. Khozyaystvo Oil Ind.* **2016**, *2016*, 96–99.
6. Cheraghian, G.; Hendraningrat, L. A review on applications of nanotechnology in the enhanced oil recovery part A: Effects of nanoparticles on interfacial tension. *Int. Nano Lett.* **2016**, *6*, 129–138. [CrossRef]
7. Yin, D.D.; Li, Y.Q.; Zhao, D.F. Utilization of produced gas of CO_2 flooding to improve oil recovery. *J. Energy Inst.* **2014**, *87*, 289–296. [CrossRef]
8. Habibi, A.; Yassin, M.R.; Dehghanpour, H.; Bryan, D. Experimental investigation of CO2-oil interactions in tight rocks: A Montney case study. *Fuel* **2017**, *203*, 853–867. [CrossRef]
9. Or, C.; Sasaki, K.; Sugai, Y.; Nakano, M.; Imai, M. Preliminary numerical modelling of CO_2 gas foaming in heavy oil and simulations of oil production from heavy oil reservoirs. *Can. J. Chem. Eng.* **2016**, *94*, 576–585. [CrossRef]
10. Shokrlu, Y.H.; Babadagli, T. Viscosity reduction of heavy oil/bitumen using micro- and nano-metal particles during aqueous and non-aqueous thermal applications. *J. Pet. Sci. Eng.* **2014**, *119*, 210–220. [CrossRef]
11. Zabala, R.; Franco, C.A.A.; Cortés, F.B.B.; Nacional, U. Application of Nanofluids for Improving Oil Mobility in Heavy Oil and Extra-Heavy Oil: A Field Test. In Proceedings of the SPE Improved Oil Recovery Conference, Tulsa, OK, USA, 11–13 April 2016.
12. Shuwa, S.M.; Jibril, B.Y. Heavy-Oil-Recovery Enhancement with Choline Chloride/Ethylene Glycol-Based Deep Eutectic Solvent. *SPE J.* **2015**, *20*, 79–87. [CrossRef]
13. Ding, F.; Gao, M. Pore wettability for enhanced oil recovery, contaminant adsorption and oil/water separation: A review. *Adv. Colloid Interface Sci.* **2021**, *289*, 102377. [CrossRef] [PubMed]
14. Jiang, R.; Li, K.; Horne, R. A Mechanism Study of Wettability and Interfacial Tension for EOR Using Silica Nanoparticles. In Proceedings of the SPE Annual Technical Conference and Exhibition, Society of Petroleum Engineers, San Antonio, TX, USA, 9–11 October 2017.
15. Wang, J.; Han, M.; Fuseni, A.B.; Cao, D. Surfactant Adsorption in Surfactant-Polymer Flooding for Carbonate Reservoirs. In Proceedings of the SPE Middle East Oil & Gas Show and Conference, Society of Petroleum Engineers, Manama, Bahrain, 8–11 March 2015.
16. Al-Hashim, H.S.; Obiora, V.; Al-Yousef, H.Y.; Fernandez, F.; Nofal, W. Alkaline Surfactant Polymer Formulation for Carbonate Reservoirs. *Pet. Sci. Technol.* **2005**, *23*, 723–746. [CrossRef]
17. Khan, M.Y.; Samanta, A.; Ojha, K.; Mandal, A. Design of Alkaline/Surfactant/Polymer (ASP) Slug and its use in Enhanced Oil Recovery. *Pet. Sci. Technol.* **2009**, *27*, 1926–1942. [CrossRef]
18. Sheng, J. *Modern Chemical Enhaced Oil Recovery*; Cambridge University Press: Cambridge, UK, 2010.
19. Abbas, A.H.; Sulaiman, W.R.W.; Jaafar, M.Z.; Gbadamosi, A.O.; Ebrahimi, S.S.; Elrufai, A. Numerical study for continuous surfactant flooding considering adsorption in heterogeneous reservoir. *J. King Saud Univ. Eng. Sci.* **2020**, *32*, 91–99. [CrossRef]
20. Chang, H.L.; Zhang, Z.Q.; Wang, Q.M.; Xu, Z.S.; Guo, Z.D.; Sun, H.Q.; Cao, X.L.; Qiao, Q. Advances in polymer flooding and alkaline/surfactant/polymer processes as developed and applied in the People's Republic of China. *JPT J. Pet. Technol.* **2006**, *58*, 84–89. [CrossRef]
21. Vargo, J.; Turner, J.; Vergnani, B.; Pitts, M.J.; Wyatt, K.; Surkalo, H.; Patterson, D. Alkaline-surfactant-polymer flooding of the Cambridge Minnelusa Field. *SPE/AAPG West. Reg. Meet.* **2000**, 1–7. [CrossRef]
22. Wu, Y.; Chen, W.; Dai, C.; Huang, Y.; Li, H.; Zhao, M.; He, L.; Jiao, B. Reducing surfactant adsorption on rock by silica nanoparticles for enhanced oil recovery. *J. Pet. Sci. Eng.* **2017**, *153*, 283–287. [CrossRef]
23. Li, S.; Torsæter, O. Experimental Investigation of the Influence of Nanoparticles Adsorption and Transport on Wettability Alteration for Oil Wet Berea Sandstone. In Proceedings of the SPE Middle East Oil & Gas Show and Conference, Society of Petroleum Engineers, Manama, Bahrain, 8–11 March 2015.
24. Dai, C.; Wang, X.; Li, Y.; Lv, W.; Zou, C.; Gao, M.; Zhao, M. Spontaneous Imbibition Investigation of Self-Dispersing Silica Nanofluids for Enhanced Oil Recovery in Low-Permeability Cores. *Energy Fuels* **2017**, *31*, 2663–2668. [CrossRef]

25. Aurand, K. *Enhanced Oil Recovery Using Silica Nanoparticles an Experimental Evaluation of Oil Production*; Norwegian University of Science and Technology: Trondheim, Norway, 2017.
26. Sharma, T.; Sangwai, J.S.J.S. Silica nanofluids in polyacrylamide with and without surfactant: Viscosity, surface tension, and interfacial tension with liquid paraffin. *J. Pet. Sci. Eng.* **2017**, *152*, 575–585. [CrossRef]
27. Youssif, M.I.; El-Maghraby, R.M.; Saleh, S.M.; Elgibaly, A. Silica nanofluid flooding for enhanced oil recovery in sandstone rocks. *Egypt. J. Pet.* **2017**, *27*, 6–11. [CrossRef]
28. Nguele, R.; Sreu, T.; Inoue, H.; Sugai, Y.; Sasaki, K. Enhancing Oil Production Using Silica-Based Nanofluids: Preparation, Stability, and Displacement Mechanisms. *Ind. Eng. Chem. Res.* **2019**, *58*, 15045–15060. [CrossRef]
29. Ogolo, N.A.; Olafuyi, O.A.; Onyekonwu, M.O. Enhanced Oil Recovery Using Nanoparticles. *Saudi Arab. Sect. Tech. Symp. Exhib.* **2012**, *9*. [CrossRef]
30. Hendraningrat, L.; Shidong, L.; Torsæter, S.; Torsæter, O. A glass micromodel experimental study of hydrophilic nanoparticles retention for EOR project. In Proceedings of the Society of Petroleum Engineers—SPE Russian Oil and Gas Exploration and Production Technical Conference and Exhibition 2012, Moscow, Russia, 16–18 October 2012; Volume 1, pp. 124–146.
31. Sharma, T.; Iglauer, S.; Sangwai, J.S. Silica Nanofluids in an Oilfield Polymer Polyacrylamide: Interfacial Properties, Wettability Alteration, and Applications for Chemical Enhanced Oil Recovery. *Ind. Eng. Chem. Res.* **2016**, *55*, 12387–12397. [CrossRef]
32. Zargartalebi, M.; Kharrat, R.; Barati, N.; Zargartalebi, A. Slightly hydrophobic silica nanoparticles for enhanced oil recovery: Interfacial and rheological behaviour. *Int. J. Oil Gas Coal Technol.* **2013**, *6*, 408. [CrossRef]
33. Hadia, N.J.; Ng, Y.H.; Stubbs, L.P.; Torsæter, O. High salinity and high temperature stable colloidal silica nanoparticles with wettability alteration ability for eor applications. *Nanomaterials* **2021**, *11*, 707. [CrossRef]
34. Rueda, E.; Akarri, S.; Torsæter, O.; Moreno, R.B.Z.L. Experimental investigation of the effect of adding nanoparticles to polymer flooding in water-wet micromodels. *Nanomaterials* **2020**, *10*, 1489. [CrossRef]
35. Cheraghian, G.; Kiani, S.; Nassar, N.N.; Alexander, S.; Barron, A.R. Silica Nanoparticle Enhancement in the Efficiency of Surfactant Flooding of Heavy Oil in a Glass Micromodel. *Ind. Eng. Chem. Res.* **2017**, *56*, 8528–8534. [CrossRef]
36. Nguele, R.; Sasaki, K. Asphaltene behavior at the interface oil-nanofluids: Implications to adsorption. *Colloids Surf. A Physicochem. Eng. Asp.* **2021**, *622*, 126630. [CrossRef]
37. Sadegh Mazloom, M.; Hemmati-Sarapardeh, A.; Husein, M.M.; Shokrollahzadeh Behbahani, H.; Zendehboudi, S. Application of nanoparticles for asphaltenes adsorption and oxidation: A critical review of challenges and recent progress. *Fuel* **2020**, *279*, 117763. [CrossRef]
38. Hendraningrat, L.; Li, S.; Torsæter, O.; Ntnu, T. Enhancing Oil Recovery of Low-Permeability Berea Sandstone through Optimized Nanofluids Concentration. *Soc. Pet. Eng.* **2013**, 713–722. [CrossRef]
39. Pei, H.H.; Zhang, G.C.; Ge, J.J.; Zhang, J.; Zhang, Q.; Fu, L.P. Investigation of Nanoparticle and Surfactant Stabilized Emulsion to Enhance Oil Recovery in Waterflooded Heavy Oil Reservoirs. In Proceedings of the SPE Canada Heavy Oil Technical Conference, Calgary, AB, Canada, 9–11 June 2015.
40. Preflush | Oilfield Glossary. Available online: https://glossary.oilfield.slb.com/en/terms/p/preflush (accessed on 1 October 2021).
41. Sheng, J.J. Alkaline Flooding. In *Enhanced Oil Recovery Field Case Studies*; Elsevier Inc.: Amsterdam, The Netherlands, 2013; pp. 143–167; ISBN 9780123865458.
42. Al-Anssari, S.; Arif, M.; Wang, S.; Barifcani, A.; Iglauer, S. Stabilising nanofluids in saline environments. *J. Colloid Interface Sci.* **2017**, *508*, 222–229. [CrossRef] [PubMed]
43. Songolzadeh, R.; Moghadasi, J. Stabilizing silica nanoparticles in high saline water by using ionic surfactants for wettability alteration application. *Colloid Polym. Sci.* **2017**, *295*, 145–155. [CrossRef]
44. Drews, A. Standard Test Method for Acid Number of Petroleum Products by Potentiometric Titration. *Man. Hydrocarb. Anal.* **2008**, *i*, 159–159-7. [CrossRef]
45. Suslick, K.S. The Chemical Effects of Ultrasound. *Sci. Am.* **1989**, *260*, 80–86. [CrossRef]
46. Yu, W.; Xie, H. A Review on Nanofluids: Preparation, Stability Mechanisms, and Applications. *J. Nanomater.* **2012**, *2012*, 435873. [CrossRef]
47. Vinogradov, J.; Jackson, M.D.; Chamerois, M. Zeta potential in sandpacks: Effect of temperature, electrolyte pH, ionic strength and divalent cations. *Colloids Surf. A Physicochem. Eng. Asp.* **2018**, *553*, 259–271. [CrossRef]
48. Bhattacharjee, S. DLS and zeta potential—What they are and what they are not? *J. Control. Release* **2016**, *235*, 337–351. [CrossRef] [PubMed]
49. Agrawal, Y.; Patel, V. Nanosuspension: An approach to enhance solubility of drugs. *J. Adv. Pharm. Technol. Res.* **2011**, *2*, 81. [CrossRef] [PubMed]
50. Ngo, I.; Sasaki, K.; Nguele, R.; Sugai, Y. Formation Damage Induced by Water-Based Alumina Nanofluids during Enhanced Oil Recovery: Influence of Postflush Salinity. *ACS Omega* **2020**, *5*, 27103–27112. [CrossRef]
51. Hendraningrat, L.; Torsæter, O. A Stabilizer that Enhances the Oil Recovery Process Using Silica-Based Nanofluids. *Transp. Porous Media* **2015**, *108*, 679–696. [CrossRef]
52. Ilyas, S.U.; Pendyala, R.; Marneni, N. Preparation, sedimentation, and agglomeration of nanofluids. *Chem. Eng. Technol.* **2014**, *37*, 2011–2021. [CrossRef]
53. Haddad, Z.; Abid, C.; Oztop, H.F.; Mataoui, A. A review on how the researchers prepare their nanofluids. *Int. J. Therm. Sci.* **2014**, *76*, 168–189. [CrossRef]

54. Zhao, M.; Lv, W.; Li, Y.; Dai, C.; Zhou, H.; Song, X.; Wu, Y. A study on preparation and stabilizing mechanism of hydrophobic silica nanofluids. *Materials* **2018**, *11*, 1385. [CrossRef]

55. Qu, J.; Wu, H. Thermal performance comparison of oscillating heat pipes with SiO 2/water and Al2O3/water nanofluids. *Int. J. Therm. Sci.* **2011**, *50*, 1954–1962. [CrossRef]

56. Ma, B.; Banerjee, D. A Review of Nanofluid Synthesis. In *Advances in Nanomaterials*; Husain, M., Khan, Z.H., Eds.; Advanced Structured Materials; Springer India: New Delhi, India, 2016; Volume 79, pp. 135–176. ISBN 978-81-322-2666-6.

57. Escrochi, M.; Mehranbod, N.; Ayatollahi, S. The gas-oil interfacial behavior during gas injection into an asphaltenic oil reservoir. *J. Chem. Eng. Data* **2013**, *58*, 2513–2526. [CrossRef]

58. Georgiadis, A.; Maitland, G.; Trusler, J.P.M.; Bismarck, A. Interfacial tension measurements of the (H_2O + n-decane + CO_2) ternary system at elevated pressures and temperatures. *J. Chem. Eng. Data* **2011**, *56*, 4900–4908. [CrossRef]

59. Bera, A.; Mandal, A.; Guha, B.B. Synergistic effect of surfactant and salt mixture on interfacial tension reduction between crude oil and water in enhanced oil recovery. *J. Chem. Eng. Data* **2014**, *59*, 89–96. [CrossRef]

60. Farhadi, H.; Ayatollahi, S.; Fatemi, M. The effect of brine salinity and oil components on dynamic IFT behavior of oil-brine during low salinity water flooding: Diffusion coefficient, EDL establishment time, and IFT reduction rate. *J. Pet. Sci. Eng.* **2021**, *196*, 107862. [CrossRef]

61. Lashkarbolooki, M.; Ayatollahi, S.; Riazi, M. The impacts of aqueous ions on interfacial tension and wettability of an asphaltenic-acidic crude oil reservoir during smart water injection. *J. Chem. Eng. Data* **2014**, *59*, 3624–3634. [CrossRef]

62. Donaldson, E.C.; Tiab, D.E.C.D.; Donaldson, E.C. *Petrophysics: Theory and Practice of Measuring Reservoir Rock and Fluid Transport Properties*, 2nd ed.; Gulf Professional Pub./Elsevier: Amsterdam, The Netherlands, 2004; ISBN 978-0-12-803188-9.

63. Mcelfresh, P.; Olguin, C.; Ector, D. The Application of Nanoparticle Dispersions to Remove Paraffin and Polymer Filter Cake Damage. In Proceedings of the SPE International Symposium and Exhibition on Formation Damage Control, Lafayette, LS, USA, 15–17 February 2012; pp. 1–7. [CrossRef]

64. Sun, X.; Zhang, Y.; Chen, G.; Gai, Z. Application of Nanoparticles in Enhanced Oil Recovery: A Critical Review of Recent Progress. *Energies* **2017**, *10*, 345. [CrossRef]

65. Aveyard, R.; Binks, B.P.; Clint, J.H. Emulsions stabilised solely by colloidal particles. *Adv. Colloid Interface Sci.* **2003**, *100–102*, 503–546. [CrossRef]

66. Snosy, M.F.; El Ela, M.A.; El-Banbi, A.; Sayyouh, H. Impact of the injected water salinity on oil recovery from sandstone formations: Application in an Egyptian oil reservoir. *Petroleum* **2021**. [CrossRef]

67. Sheng, J.J. Critical review of low-salinity waterflooding. *J. Pet. Sci. Eng.* **2014**, *120*, 216–224. [CrossRef]

68. Alomair, O.A.; Matar, K.M.; Alsaeed, Y.H. Nanofluids application for heavy oil recovery. In Proceedings of the SPE Asia Pacific Oil & Gas Conference and Exhibition, Adelaide, Australia, 14–16 October 2014.

69. Kazemzadeh, Y.; Eshraghi, S.E.; Kazemi, K.; Sourani, S.; Mehrabi, M.; Ahmadi, Y. Behavior of asphaltene adsorption onto the metal oxide nanoparticle surface and its effect on heavy oil recovery. *Ind. Eng. Chem. Res.* **2015**, *54*, 233–239. [CrossRef]

70. Hendraningrat, L.; Engeset, B.; Suwarno, S.; Li, S.; Torsæter, O. Laboratory investigation of porosity and permeability impairment in Berea sandstones due to hydrophilic nanoparticle retention. In Proceedings of the International Symposium of the Society of Core Analysts, Napa Valley, CA, USA, 16–19 September 2013; pp. 16–19.

71. Feia, S.; Dupla, J.C.; Ghabezloo, S.; Sulem, J.; Canou, J.; Onaisi, A.; Lescanne, H.; Aubry, E. Experimental investigation of particle suspension injection and permeability impairment in porous media. *Geomech. Energy Environ.* **2015**, *3*, 24–39. [CrossRef]

72. Zamani, A.; Maini, B.; Pereira-Almao, P. Flow of nanodispersed catalyst particles through porous media: Effect of permeability and temperature. *Can. J. Chem. Eng.* **2012**, *90*, 304–314. [CrossRef]